# Chemical mapping of the degradation of geranium lake in paint cross sections by MALDI-MSI

# Chemical Mapping of the degradation of geranium lake in paint cross sections by MALDI-MSI

Alba Alvarez-Martin[1,2,3*], Jusal Quanico[4], Teresa Scovacricchi[1], Ermanno Avranovich Clerici[1], Geert Baggerman[4], Koen Janssens[1,2]

[1]AXIS, NANOLab Centre of Excellence, Department of Physics, University of Antwerp, 2020 Antwerpen, Belgium;

[2]Conservation and Science, Rijksmuseum Amsterdam, 1071 ZC Amsterdam, The Netherlands;

[3] Royal Museum for Central Africa, 3080 Tervuren, Belgium;

[4]Center for Proteomics, University of Antwerp, 2020 Antwerpen, Belgium

*Corresponding author: Alba Alvarez-Martin. A.Alvarez.Martin@rijksmuseum.nl*

## ABSTRACT

Matrix Assisted Laser Desorption Ionization - Mass Spectrometry Imaging (MALDI-MSI) has become a powerful method to extract spatially resolved chemical information in complex materials. This study provides the first use of MALDI-MSI to define spatial-temporal changes in oil paints. Due to the highly heterogeneous nature of oil paints, the sample preparation had to be optimized to prevent molecules from delocalizing. Here, we present a new protocol for the layer-specific analysis of oil paint cross-sections achieving a lateral resolution of 10 µm and without losing ionization efficiency due to topographic effects. The efficacy of this method was investigated in oil paint samples containing a mixture of two historic organic pigments, geranium lake and lead white, a mixture often employed in the oeuvre of the painter Vincent Van Gogh. This methodology not only allows for spatial visualization of the molecules

responsible for the pink hue of the paint, but it also helps to elucidate the chemical changes behind the discoloration of paintings with this composition. The results demonstrate that this approach provides valuable molecular compositional information on the degradation pathways of pigments in specific paint layers and their interaction with the binding medium and other paint components and with light over time. Since a spatial correlation between molecular species and the visual pattern of discoloration pattern can be made, we expect that mass spectrometry imaging will become highly relevant in future degradation studies of many more historical pigments and paints.

## INTRODUCTION

Since ancient times, pigments have been used by artists to portray light, colour and depth in paintings. However, during the lifetime of an artwork, pigments may be subject to molecular alterations that can lead to a gradual loss of brightness and intensity of the original colour, sometimes altering the artwork's appearance from the artist's original intent .

Recent examples of these degradation processes are (a) the degradation of cadmium sulfide-based oil paints in *The Scream* by Edvard Munch, [1] (b) the darkening of cadmium yellow in works by Picasso, [2] (c) the degradation of arsenic containing pigments such as the yellow orpiment and orange-red realgar in still life paintings by Nellius, Mignon and De Heem, [3-5] (d) the discoloration of chrome yellow, bleaching of read lead and red lakes in numerous Van Gogh paintings, [6-9] (e) the ultramarine sickness in works by Vermeer and Jan Steen[10, 11] involving a blackening of the blue paint or (f) the discoloration of smalt (another blue pigment) in Rembrandt paintings. [12]

To understand the original palette used by artists, a full characterization of all materials used in their paintings, and their molecular changes over time, is needed in most cases. For this aim, major advances in non-invasive spectroscopic methods have been realized in the last decade. To obtain improved insight into the deterioration of inorganic pigments and their associated reaction mechanisms, several powerful methods were developed and optimized, both for imaging analysis of complete works of art or of minuscule paint fragments. [13] On the other side, the non-invasive detection of organic pigments by spectroscopic techniques is possible but hard to achieve when the original pigment has degraded or is present at a very low concentration. Mass spectrometry (MS) has contributed significantly not only to the identification of historical and modern organic pigments in artworks, [14-18] but also to the characterization of the waxes, lipids, varnishes and protein paint binders. [19] However, it usually requires small samples of the artifacts to be consumed. In addition, sample preparation methodology required for traditional

MS techniques such as liquid or gas chromatography, usually implies the dissolution of the spatial distribution pattern of the pigment within the paint sample (and its various layers) under investigation.

New approaches using ambient MS techniques have contributed significantly to the identification of organic pigments and binding media. [20-23] The fundamental aspects of ambient MS involve the direct sampling and ionization of analytes from the sample under ambient condition and with minimal sample preparation. However, in view of the use of solvents (in Desorption Electrospray Ionization, DESI and Surface Acoustic Wave Nebulization, SAWN) or the large spot size of the (Direct Analysis in Real Time, DART) ionization source, these techniques still require significant development in order to be able to map the distribution of pigments within minuscule cross-sectioned paint samples. To that end, a third branch of mass spectrometry appears to have much more potential at present: Matrix Assisted Laser Desorption Ionization (MALDI)-Mass Spectrometry Imaging (MSI).

MALDI-MSI is a cutting-edge MS-based method that can visualize the two-dimensional distribution of molecules without requiring extraction, purification, and separation operations to be performed on the sample material. After collecting a mass spectrum at one spot by localized laser excitation, the sample is moved to illuminate another position, until the entire sample is scanned in a raster format. By choosing a selection of masses in the resulting spectra that corresponds to the studied analyte, the data can be used to map its distribution across a cross-sectioned multi-layered sample. This results in images of the distribution of these masses with a lateral resolution that can be as low as 1-2 µm, depending on the analyte, sample preparation, matrix and instrument employed. While already an extensive literature exists on MS imaging of peptides, proteins, lipids and carbohydrates in the biomedical field, [24-27] studies of imaging of organic pigments in cultural heritage related samples are currently scarce and, to the best of our knowledge, are non-existent for the case of multi-layered oil paint samples.

Sample handling and preparation protocols for MSI need to ensure that analytes can be extracted, ionized and analysed without changing their geometrical location. This is necessary optimally visualize and understand the behaviour of analytes in their real environment. Traditional protocols for MALDI-MSI, such as cryo-sectioning of snap-frozen or embedded samples followed by thaw mounting or gluing methods, have proven their value in the context of tissue and bone imaging analysis. [28] However, due to the granulated structure, the heterogeneous morphology and variable solubility of the components of (historical) paints these sample preparation protocols cannot be simply transferred when performing MSI analysis of multi-layered paint samples. Therefore, it was necessary to develop and validate a workflow compatible with the complex nature of oil paints without causing the delocalization of analytes, a non-desirable phenomenon in MSI.

As oil paintings consist of a mixture of pigments of quite different nature and chemical reactivity, several chemical degradation phenomena may spontaneously and simultaneously take place as a function of time. The efficacy of MALDI-MSI method was investigated in oil paint samples containing a mixture of two historic organic pigments: the organic-based pigment eosin (aka geranium lake) and the inorganic-based pigment lead white.

Geranium lake is formed by the precipitation of an organic dye (eosin) onto a metal (aluminium or lead) salt. In the late 19th century, the beginning of Modern Art and a period of tremendous change for both oil painters and watercolourists, geranium lake became commercially available in oil paint tubes. At this moment, Vincent Van Gogh (1853−1890), the most well-known Dutch post-impressionist artist, started introducing this new colour in his palette, hereby giving his artworks a much more vibrant appearance that before. [29] Despite its brightness, geranium lake tends to rapidly fade leading to the discoloration of masterworks within Van Gogh's lifetime, as he reported in his letters[30] *"You were right to tell Tasset that the geranium lake should be included after all, he sent it, I've just checked — all the colours that Impressionism*

*has made fashionable are unstable, all the more reason boldly to use them too raw, time will only soften them too much"* (*letter 595*).

The overall goal of this study is to deepen the knowledge of the use of geranium lake in the avant-garde artistic community of the late 19th century. Accordingly, it was decided to create a series of paint models capable of simulating and reproducing the characteristics of a pictorial layer. Within the series, the composition and concentration of geranium lake, other inorganic pigments and the binder (linseed oil) were varied. These model paints were not only intended to investigate the degradation behaviour of the eosin molecule but also to study its behaviour in the presence of other materials that are typically present within paintings by Van Gogh and contemporary artists. Therefore, as inorganic component of the model paints, lead white was selected as it is one of the most commonly used white pigments from ancient times until 19th century. [31] Van Gogh created paler tints of red and pink by mixing red lakes with varying amount of white pigments, including lead and zinc whites. [29, 32]

The discoloration mechanism of eosin has been documented, in solution and oil paint models, [23, 33-36] showing that eosin exhibits a multistep degradation process; where initially a debromination takes place, while the chromophore remains essentially intact, further degradation steps lead to the breakdown of the chromophore responsible for the red-pink colour. This multi-step degradation mechanism resembles the photodegradation of other organic dyes such as Rhodamine B, in which the subsequent loss of N-ethyl functional groups takes place before the cleavage of the chromophore and subsequent mineralization. [37] An analogous situation has been found in the context of inorganic pigments where vermilion, a mercury-based red pigment used by artists since antiquity, undergoes a series of irreversible phase conversions, resulting in the darkening of the original red colour. [38] The degradation mechanism of vermilion in paint layers has been elucidated via secondary ion mass spectrometry (SIMS), femtosecond pump-probe optical microscopy and various synchrotron-

based microscopic techniques, such as X-ray diffraction (XRD), X-ray fluorescence (XRF) or X-ray absorption near edge spectroscopy (XANES). [38-40] The visualization of the distribution of the inorganic degradation products and their co-localization in the paint proved to be highly relevant to gain deeper chemical insight into colour changes. However, the molecular mapping of organic pigments, and their breakdown products within the individual layers of (cross sectioned) paint samples remains a challenge. While attenuated total reflection-Fourier transform infrared (ATR-FTIR) microscopy is able to map functional groups, it lacks the specificity needed to follow the subtle molecular changes associated with colour change. [41]

Thus, the specific aim of this study has been to seek evidence that the temporal multi-step degradation process of geranium lake can also be experimentally observed in a more direct manner by recording the spatial distribution of the original eosin molecule and its by-products in oil paint cross-sections during photo-aging using MALDI-MSI.

## MATERIALS AND METHODS

**Chemicals.** Eosin-Y (99% dye content), 2,5-dihydroxybenzoic acid (DHB), norharmane (NRM) and aluminium chloride hexahydrate ($AlCl_3 \cdot 6H_2O$) were purchased from Sigma-Aldrich (Darmstadt, Germany). Cerussite was purchased as pure lead carbonate $PbCO_3$ from Acros organics (Molinons, France). The bleached linseed oil employed to prepare the paints was purchased from Royal Talens (Apeldoorn, The Netherlands), and a new bottle was opened exclusively for this study. Conductive indium/tin oxide-coated slides (ITO) and Peptide Mix 6 calibration standard were purchased from LaserBioLabs (Sophia-Antipolis, France). Phosphorous red clusters were purchased from (Sigma-Aldrich (Darmstadt, Germany). Conductive carbon tapes AGG3347N and AGG3347A were purchased from Agar Scientific Ltd (London, UK).

**Synthesis of Geranium Lake and Lead White, Oil Paint Models Preparation and Artificial Photoaging.** The synthesis of the geranium lake was carried out, using eosin Y as a precursor, according to the protocol proposed by Claro et al. [42] The synthesis and characterization of lead white was conducted as described in Supplementary Information. In order to present a systematic methodology for the sample preparation, the oil absorption value (OA) was calculated for each pigment as indicated in **Table S1**. Oil paint models were prepared by mixing geranium lake, lead white and linseed oil in the proportions indicated in **Table S2**. The resulting mixture was scattered with a paint applicator on transparent PVC film with a 500 µm thickness. Oil paints were allowed to dry in the dark at room temperature and with air circulation for four weeks. Once the surface was dry-to-touch, samples were subjected to natural light aging up to 107 days. During the aging, the temperature and relative humidity fluctuated between 20-25 °C and 60-70% respectively. Unaged samples were kept in dark until the analysis and were considered as control samples. Oil paint samples corresponding to time 0 (control), 7, 40 and 107 days were included in this study.

**Microscopy.** A Nikon Eclipse LV100 microscope was employed to collect micrometric pictures. All the images were acquired in transmission mode using a dark-field technique to enhance the chromatic contrast of the degraded regions in the thin sections. The light source of the microscope was a halogen 12V50W halogen lamp. Multifocal pictures were acquired with the NIS-Elements D 5.30.01 software and the TANGO-Desktop high-resolution stepper motor controller.

**X-Ray Powder Diffraction (XRPD)**. The instrument employed for this analysis was a self-built XRPD setup operated in reflection geometry employing a monochromatic copper source IμS (Incoatec, Geesthacht, Germany; Cu-Kα: 8.04 keV) [43]. The X-Ray tube was operated at 50 kV and a current of 1000 μA with a beam spot probing the sample with sizes of 1 x 0,3 $mm^2$. A planar imaging detector (Pilatus 200K, Dectris, Villigen, CH) was employed to collect diffraction patterns, the acquisition time per analysed spot was set to 10 seconds. The final patterns, used for semi-quantification of the crystalline phases, were a result of 10 diffractograms collected at different point and averaged together. The two-dimensional (2D) X-ray patterns collected from each sample were azimuthally integrated to one-dimensional (1D) diffractograms employing XRDUA a software developed in the University of Antwerp. [44] The crystalline phases in the 1D pattern were identified by comparing the data with a powder diffraction database, taking into account the observed diffraction peak positions (2θ angles) and their relative intensities. After azimuthal integration, fitting was performed on the 1D diffractograms using a Rietveld model containing the information to allow semi-quantitative analyses.

**Fiber Optics Reflectance Spectroscopy (FORS)**. The instrument consists of an Avalight-HAL light source, Avantes fiber optics cables with small tip probe and 45° probe holder, an AvaSpec-2048 spectrometer and Avasoft2 software for spectrum readout.

**Matrix application**. Matrix application using sublimation was preferred as the sublimation process occurs under vacuum and the ITO slide is constantly cooled using an ice-cooling system. These conditions prevent molecules from delocalizing. [45] The matrix was sublimated onto the cross sections at 140 ºC for 13 min using a sublimator (Thermo) set up in-house, [46] which leads to an average of 0.424 mg matrix deposited per $cm^2$ based on three independent measurements.

**MALDI-MSI.** MS imaging of cross sections was performed using a rapiflex MALDI-TOF instrument (Bruker Daltonics, Bremen, Germany). Images were acquired at 10-µm resolution scanning at *m/z* 300-2000 with the Smartbeam 3D laser (355 nm) firing at a frequency of 10 kHz. Each spectrum was recorded after accumulating 500 laser shots per spot. The ion source voltage was set to 20 kV, while the PIE and lens were at 2.570 and 11.600 kV, respectively. The reflectors were set at 20.800, 1.085 and 8.700 kV. Matrix suppression by deflection up to *m/z* 240 was activated. The reflector detector gain, and sampling rate were kept constant on all imaging acquisitions. External calibration in both positive and negative modes were performed using Peptide Mix 6 calibration standard and phosphorous red clusters respectively.

**Data analysis.** The acquired MS images were uploaded in SCiLS Lab version 2016b (Bruker Daltonics). The baseline was removed using the top hat method. The ion distributions of the pigments were mapped by plotting the signal intensities in all spectra normalized against the total ion count. Subsequently, orthogonal matching pursuit (OMP) was used to detect peaks; these peaks were aligned to the mean spectrum by centroid matching and automatic spatial segmentation was performed by using the bisecting k-means algorithm with Manhattan as the distance metric followed by application of weak hotspot removal. These ion distributions were plotted at ±0.300 Da *m/z* intervals, with the masses reported as the maximum value in each interval. A first overview of the spatial regions of the eosin molecule (using the isotopic peak at *m/z* 648.37) was achieved by applying hierarchical clustering on the MSI data of images of

paint samples containing 100%, 95%, 50% and 5% in weight of geranium lake (**See Table S2**). The depth of clustering was selected interactively. Receiver Operating Characteristic (ROC) analysis was performed to detect *m/z* values which discriminate between samples containing 100% and 5% in weight of geranium lake and vice versa, with AUCs $\geq$ 0.75 considered significant.

## RESULTS AND DISCUSSION

During artificial photoaging of the eosin/lead white paints,, FORS and optical microscopy were used to follow the discoloration process observed on the surface of the paint models (**Figure 1A-B**). When geranium lake (GL) is the only pigment in the paint, (lowest curve in **Figure 1A**; leftmost column in **Figure 1B**), hardly any colour changes are observed on the surface exposed to light aging. Nevertheless, when GL is mixed with lead white, a gradually discoloration is observed versus time (**Figure 1B**). The same trend was observed in our previous studies, [47] where the presence of lead white appears to stimulate the discoloration rate which is measured as an increase of total colour change (ΔE*) (**Figure 1A**). When considering the degraded paints in cross-section, as shown in **Figure 1C**, a clear discoloration of the top layer, next to a less pronounced colour change throughout the aged samples is observed as a function of aging time. However, the spectroscopic techniques previously employed were unable to elucidate molecular changes below the degraded outermost surface and could not provide information about the spatial distribution of secondary products within the sample. Therefore, to monitor the chemical changes occurring during the discoloration process and to visualize the lateral distribution of degradation products, these oil paint cross sections were examined at multiple times during their light aging by MALDI-MSI.

**Optimization of ionization yields.** In order to detect low abundance and low molecular weight molecules, two matrices were investigated in this study, 2,5-dihydroxybenzoic acid (DHB) and norharmane (NRM). Both matrices were prepared in the same way:10 mg of matrix material was dissolved in 1 mL 70% acetonitrile/0.1% trifluoroacetic acid. Ionization was tested in negative and positive mode for both matrices. For method optimization the synthetized geranium lake (aluminium complex) and its pure precursor, eosin Y, were dissolved in 50 µL of ethanol. Then, 5 µL of these solutions were mixed with 5 µL of matrix, and 1 µL was spotted on the MALDI target plate after which a molecular profile was obtained. The peaks associated

with the single tetra-brominated monomeric eosin were only observed with DHB at *m/z* 648.23 ($[C_{20}H_9O_5Br_4]^+$) and *m/z* 646.74 ($[C_{20}H_7O_5Br_4]^-$), in positive and negative mode respectively (**Figure S2** and **S3**), achieving the best results in positive mode.

**Sample Preparation Optimization for MALDI-MSI.** To preserve the spatial accuracy of MALDI-MSI, it is required that the cross section maintains the original structure of the parent material.. Thus, to investigate spatial alterations during the sample preparation, different approaches were adapted to the specific nature and properties of oil paint samples. The first attempt was to freeze and section the oil paint on/with a microtome and thaw mount it on an ITO (Indium Tin Oxide)-coated slide. However, part of the organic pigment became solubilized during this procedure, creating a coloured halo around the sample, even visible even to the naked eye. The second approach was to test different embedding materials commonly used in conservation practice. Seven types of resins were tested: Technovit 2000LC, Technovit 5000, Technovit 4004, Acrifix Liquid and VersoCit-2 Liquid. Similar as in the previous attempt, paint samples displayed a diffusion of coloured particles in all embedding media tested. Although the embedding method was initially selected for its compatibility with other non-destructive analyses that could be done prior to MSI (e.g. Raman, FTIR, µ-XRF, µ-XRPD and SEM imaging), the delocalization of the analyte produced during embedding prevented us to establish the original spatially distribution of the pigment within the sample, making this modus operandi not compatible with MSI.

Microtoming of non-embedded pant samples, as illustrated in ***Scheme 1***, was then chosen to prevent delocalization of the pigment molecules in the cross section. Cracking during sectioning was avoided by protecting the sample with a thin sheet of PVC. Four paint sample thicknesses (20, 15, 10 and 5 µm) were tested. The sample thicknesses of 20 and 15 µm generated differences in the z-axis position leading to fluctuations in the signal intensities. On the other hand, samples with a thickness of 5 µm were prone to crack during the mounting.

Thus, the best compromise was achieved employing a sample thickness of 10 µm. In addition, two conductive tapes, a carbon tape and an aluminium-core carbon tape, were evaluated with the aim to minimize topography effects of the sample that can lead the defocusing of the laser at the sample surface. **Figure S4** shows the optical image of a sample placed on top of both types of conductive tapes. Unlike the porous surface of the conventional carbon tape (**Figure S4A)**, which leads to defocusing of the laser at the sample surface, the aluminium-core based tape has a smoother surface (**Figure S4B)**. This improvement in topography translated into a drastic improvement of the acquired spectrum when mounted on an aluminium-core conductive tape.

To avoid differences in sample height (along the z-axis) may cause fluctuations in ionization and shifts in signal intensity, the calibrant was also spotted on the conductive tape to maintain the same sample height overall during calibration. To minimize technical variability, for each paint sample, six cross sections were mounted in pairs on three conductive pieces of tape on the same ITO slide (see ***Scheme 1***). Finally, matrix deposition was carried out by sublimation as described in the Methods section.

Matrix application using sublimation was preferred over spray deposition as it is completely solvent-free and the process occurs under vacuum. Therefore, the analytes within the sample can never become resolubilized, preventing the delocalization of molecules. [48, 49] It also enabled to perform MS imaging at higher spatial resolution since the resulting matrix crystals were smaller (ca. 0.2 - 1 µm diameter) [46, 50] than the laser spot size (of the order of 10 x 10 µm) used during the experiments.

**MS Imaging on paint cross sections**. The sample preparation method discussed above was evaluated to investigate the molecular changes to geranium lake (GL) that the combined presence of light and lead white (LW) may cause. Thus, three replicate sets of each GL-LW mixture (100. 95, 50 and 5% of GL in weight, see **Table S2 and Figure 1B**) were imaged by MALDI-MSI after 0 (control), 7, 40 and 107 days of light aging. MALDI-MSI spectral data of all samples presented the characteristic isotopic pattern of the tetrabrominated eosin monomer at *m/z* 648.37 ($[C_{20}H_9O_5Br_4]^+$), accompanied by the peaks associated with the tri-brominated and non-brominated eosin forms at *m/z* 568.56 ($[C_{20}H_{10}O_5Br_3]^+$) and 332.63 ($[C_{20}H_{13}O_5]^+$, aka fluorescein) respectively (**Figure 2A**), together with their K and Na adducts. These signals were assigned by comparison with data reported previously, [23, 51] analysing their isotopic patterns and distributions, and evaluating the possible additions to the most intense and monoisotopic ions based on mass differences. As GL was widely used by Van Gogh, its degradation pathway has been extensively investigated in solution and mock-up samples. [34, 36, 52-55] These studies have revealed that an intermediate mechanism can be associated to the debromination process of the eosin molecule before leading to the breakdown of the xanthene moiety that causes total discoloration. [35, 51, 56] The ability to perform distribution analysis of the intact eosin monomer and its known degradation products on paint cross sections was evaluated next. 10 µm spatial resolution ion images of these characteristic ions in samples GL100 and GL50 are presented in **Figure 2B-C. Figure S5** contains the ion images of all investigated samples and the monitoring of their abundance is presented in Supporting Information (**Figure S7-9**)**.** The ion images show that the molecular composition changes throughout the aging time in all studied samples. It is observed that the patterns of the parent compound (containing four Br) and its tri-brominated form are significantly different than the completely debrominated secondary product. While the intensity of the signals at *m/z* 648.37 (4-brominated eosin) and *m/z* 568.56 (3-brominated eosin) remains constant, *m/z* 332.63 (fluorescein) shows a high

intensity in the upper layer during the aging, suggesting that this molecule corresponds to a photo-reaction product. It is noteworthy that non discoloration is observed in GL100 even the abundance of the parent compound in the bulk sample decreases over time (optical images in **Figure 2B**). The preservation of the red hue is explained by the possibility that some degradation products are still preserving the chromophore moiety. While no colour changes are observed in GL100, GL95, GL50, the sample containing the highest ratio of LW (GL5 in **Figure S5**) shows a noticeable discoloration in the upper few micrometres of the paint, where no xanthene-based products are detected .

Next, we set out to evaluate how the intensities changed as function of light . By monitoring the average abundance of the eosin monomer (*m/z* 648.37 ± 0.4 Da) in the bulk sample, it is clear that this species decreased during light exposure as shown in **Figure S7**, and this effect becomes more pronounced with increasing the lead ratio in the paint. The photocatalytic potential of lead white during the degradation of geranium lake has been widely investigated showing the enhancement of the degradation of eosin when semiconductor particles were present. [57, 58] The disappearance of the chromophore moiety, responsible for the red hue, translates into the gradual loss of colour as can be visually observed in **Figures 1B and 2B**. A similar trend in signal intensity is observed for the tri-brominated eosin form at *m/z* 568.56 (**Figure S8**).

On the contrary, **Figure S9** indicates that the abundance of fluorescein generally increases under light irradiation. While this molecule appears to be most efficiently generated in GL100 to GL50, The trend presented in GL5, highest ratio of lead white, (**Figure S9**) shows a modest decrease within the time window investigated. This may indicate the simultaneous occurrence of formation and degradation of these species. It is clear here that when lead white is present in a high LW:GL ratio, the cleavage of the chromophore occurs so fast that a decrease in the intermediate compound, fluoresceine, is also observed. Interestingly, **Figure S9** also shows

that fluoresceine is present in the unaged samples, showing that it is already being produced during the drying of the oil paint. This confirms the low stability of geranium lake since its degradation already begins during the drying process, and it is catalysed by light irradiation and lead white. This result is consistent with our previous studies, where we already detected the generation of fluoresceine, via the debromination mechanism of eosin species, during drying of oil paint samples by DART-HRMS and DI-ESI-HRMS. [51]

It should be noted that the di- or mono- debrominated species, detected in our previous studies with DART- and ESI-HRMS, were not detected by MALDI-MSI. The trend previously observed of these intermediates[23] indicated the rapid and simultaneous occurrence of their formation and degradation during light aging. Another explanation might be the high resolution detector previously used (LTQ Orbitrap Velos) along with the low concentrations in which these species are present in the samples, making the detection difficult with a TOF detector. Likewise, the detection of the degradation products after the cleavage of the chromophore were not identified as their mass overlap with lead aggregates that are more abundant on the spectra. However, the analysis of the sample after solvent extraction and further analysis via SYNAPT-HRMS revealed the presence of a fragment identified at *m/z* 430.89 in the degraded samples (**Figure S10**). A suitable matrix for these specific (low molecular) compounds and an increase in the resolution system should be taken into account in a follow-up investigation in order to minimize background interferences in the low m/z range. [59]

The superposition of the three representative ions (*m/z* 648.37, *m/z* 568.56 and *m/z* 332.63) in **Figure 3A-B** reveals that their colocalization is significantly different at the light-exposed surface than in the bulk and that it evolves with increasing exposure to light. **Figure 3C-D** show the average signal intensity of these ions as a function of depth in the cross section of samples GL100 (only eosin, no lead white) and GL50 (50:50 mixture). The average signal intensity was determined from the average mass spectra of 4 to 6 region in the samples (see

**Figure S6**). In both samples the intensity of *m/z* 648.37 and *m/z* 568.56 do not change significantly with depth vs. aging time. In general, the concentration-depth curves of these two ions showed an overall trend with a small variation indicating the homogeneity within the layers.

However, in the case of *m/z* 332.63, the sample exposed to light during 107 days shows an intensity gradient from high intensity near the top of the sample with decreasing intensity towards the non-exposed areas. This confirms the formation of this degradation product at the light-exposed side of the sample. This is in agreement with the images presented in **Figure 3A-B** where *m/z* 332.63 is located in the top of the sample and *m/z* 648.37 and *m/z* 568.56 are localized across the entire cross section.

As the fully debrominated product (*m/z* 332.63) is also detected in the sample without LW, this may indicate that the loss of bromine is initiated by the light and presence of oxygen as suggested in previous studies modelling the degradation of eosin in aqueous solution. [34, 36] The mapping of this ion in a solid sample provides for first time direct evidence of this phenomenon, where eosin loses bromine before the cleavage of the chromophore.

## CONCLUSIONS

The method described in this paper allowed us to assess the spatial distribution of an historical organic pigment, geranium lake, and its degradation products in oil paints, providing the opportunity of a more complete chemical understanding of the degradation mechanism.

Due to the nature of oil paints, the traditional sample preparation for MALDI-MSI had to be modified and optimized to prevent molecules from delocalizing. Mounting was a critical step as the embedding material can solubilize or degrade the organic pigment. The combination of an appropriate sample thickness, conductive support and solvent-free matrix deposition presented in here is sufficient to provide a reproducible signal. We show that this preparation method can be applied to oil paint samples containing a mixture of organic and inorganic pigments without the need to embed the sample, while avoiding dilution and suppression effects. Hence, this new protocol enables the imaging of 10 µm thin-paint-cross-sections, allowing the monitoring of the chemical changes associated to pigment discoloration, while achieving a lateral resolution of 10 µm and without losing ionization efficiency due to topography effects.

After optimizing the sample preparation for MALDI-MSI, its validation required analysing, processing and understanding a large number of paint samples, exposed to light aging for variable lengths of time. The approach used to analyse the recorded data set obtained in this study was the manual inspection and selection of already known mass peaks, followed by the visual examination of molecular distribution images at the selected *m/z* values. This straightforward approach allowed us to find molecular masses associated to the original pigment molecule and for the first time made their spatial localization possible at different depths below the of the sample. The data generated with MALDI-MSI in this study reveals that the pattern of secondary products is significantly different at the light-exposed paint surface than in the bulk and that it evolves with aging time.

The monitoring of fluoresceine over time shows that at first, this molecule is predominantly generated in the upper layers of the sample, where the intensity of the light is the highest. However, with time, gradually also in the deeper layers this degradation product is formed. This result is consistent with our previous studies, where we observed that eosin presents a tendency to lose bromine in the presence of light, and that this phenomenon is catalysed by the semiconductor pigment lead white. Here we report for first time the clear visual confirmation between the loss of bromine due to the light exposure and the discoloration process of geranium lake in an oil-based medium. The colour change observed in the oil paint samples analysed in this study shows similarities with the discoloration phenomena visible in a number of Van Gogh paintings, where geranium lake was mixed with white pigments to create shades of pink. [29, 60-64]

By monitoring these changes with high resolution mass spectrometry imaging, we can offer for first time an explanation of the gradual discoloration process that takes places over the lifetime of a painting.

Since correlation between molecular species and colour change can be achieved, we expect that this methodology will significantly enhance the value of MALDI-MSI for artwork degradation studies. The spatial mapping of intact pigments in oil paint cross sections has the potential to revolutionize the field of cultural heritage by providing opportunities for the interrogation of degradation mechanisms not focused solely on the analysis of pigments, but also of other organic artistic materials such as oils, varnishes, waxes or materials of biological origin like egg yolk, blood or other proteinaceous materials, leading to a deep understanding of the interaction between them over the life time of a painting.

## ASSOCIATED CONTENT

Supporting information: Lead white synthesis and characterization, sample preparation, optimization of ionization yields, extended MSI results, comparison of relative intensities, SYNAPT-HSMS spectrum.


## ACKNOWLEDGMENTS

This project has received funding from the European Union's Horizon 2020 research and innovation programme under grant agreement no 891714. Authors would acknowledge financial support from the University Research Fund (BOF, UAntwerp) under project no FFB220025.

(1) Monico, L.; Cartechini, L.; Rosi, F.; Chieli, A.; Grazia, C.; De Meyer, S.; Nuyts, G.; Vanmeert, F.; Janssens, K.; Cotte, M.; et al. Probing the chemistry of CdS paints in The Scream by in situ noninvasive spectroscopies and synchrotron radiation x-ray techniques. *Science Advances* **2020**, *6* (20), eaay3514. DOI: doi:10.1126/sciadv.aay3514.
(2) Comelli, D.; MacLennan, D.; Ghirardello, M.; Phenix, A.; Schmidt Patterson, C.; Khanjian, H.; Gross, M.; Valentini, G.; Trentelman, K.; Nevin, A. Degradation of Cadmium Yellow Paint: New Evidence from Photoluminescence Studies of Trap States in Picasso's Femme (Époque des "Demoiselles d'Avignon"). *Anal. Chem.* **2019**, *91* (5), 3421-3428. DOI: 10.1021/acs.analchem.8b04914.
(3) Simoen, J.; De Meyer, S.; Vanmeert, F.; de Keyser, N.; Avranovich, E.; Van der Snickt, G.; Van Loon, A.; Keune, K.; Janssens, K. Combined Micro- and Macro scale X-ray powder diffraction mapping of degraded Orpiment paint in a 17th century still life painting by Martinus Nellius. *Herit. Sci.* **2019**, *7* (1), 83. DOI: 10.1186/s40494-019-0324-4.
(4) Keune, K.; Mass, J.; Mehta, A.; Church, J.; Meirer, F. Analytical imaging studies of the migration of degraded orpiment, realgar, and emerald green pigments in historic paintings and related conservation issues. *Herit. Sci.* **2016**, *4* (1), 10. DOI: 10.1186/s40494-016-0078-1.
(5) De Keyser, N.; Broers, F.; Vanmeert, F.; De Meyer, S.; Gabrieli, F.; Hermens, E.; Van der Snickt, G.; Janssens, K.; Keune, K. Reviving degraded colors of yellow flowers in 17th century still life paintings with macro- and microscale chemical imaging. *Science Advances* **2022**, *8* (23), eabn6344. DOI: doi:10.1126/sciadv.abn6344.
(6) Vanmeert, F.; Hendriks, E.; Van der Snickt, G.; Monico, L.; Dik, J.; Janssens, K. Chemical Mapping by Macroscopic X-ray Powder Diffraction (MA-XRPD) of Van Gogh's Sunflowers: Identification of Areas with Higher Degradation Risk. *Angew. Chem. Int. Ed. Engl.* **2018**, *57* (25), 7418-7422. DOI: 10.1002/anie.201713293.
(7) Monico, L.; Janssens, K.; Hendriks, E.; Vanmeert, F.; Van der Snickt, G.; Cotte, M.; Falkenberg, G.; Brunetti, B. G.; Miliani, C. Evidence for Degradation of the Chrome Yellows in Van Gogh's Sunflowers: A Study Using Noninvasive In Situ Methods and Synchrotron-Radiation-Based X-ray Techniques. *Angew. Chem. Int. Ed.* **2015**, *54* (47), 13923-13927. DOI: https://doi.org/10.1002/anie.201505840.
(8) Centeno, S. A.; Hale, C.; Carò, F.; Cesaratto, A.; Shibayama, N.; Delaney, J.; Dooley, K.; van der Snickt, G.; Janssens, K.; Stein, S. A. Van Gogh's Irises and Roses: the contribution of chemical analyses and imaging to the assessment of color changes in the red lake pigments. *Herit. Sci.* **2017**, *5* (1), 18, journal article. DOI: 10.1186/s40494-017-0131-8.
(9) Dooley, K. A.; Chieli, A.; Romani, A.; Legrand, S.; Miliani, C.; Janssens, K.; Delaney, J. K. Molecular Fluorescence Imaging Spectroscopy for Mapping Low Concentrations of Red Lake Pigments: Van Gogh's Painting The Olive Orchard. *Angew. Chem. Int. Ed. Engl.* **2020**, *59* (15), 6046-6053. DOI: 10.1002/anie.201915490 From NLM.
(10) van Loon, A.; Gambardella, A. A.; Gonzalez, V.; Cotte, M.; De Nolf, W.; Keune, K.; Leonhardt, E.; de Groot, S.; Proaño Gaibor, A. N.; Vandivere, A. Out of the blue: Vermeer's use of ultramarine in Girl with a Pearl Earring. *Herit. Sci.* **2020**, *8* (1), 25. DOI: 10.1186/s40494-020-00364-5.
(11) Schnetz, K.; Gambardella, A. A.; van Elsas, R.; Rosier, J.; Steenwinkel, E. E.; Wallert, A.; Iedema, P. D.; Keune, K. Evidence for the catalytic properties of ultramarine pigment. *J. Cult. Herit.* **2020**, *45*, 25-32. DOI: https://doi.org/10.1016/j.culher.2020.04.002.
(12) van Loon, A.; Noble, P.; de Man, D.; Alfeld, M.; Callewaert, T.; Van der Snickt, G.; Janssens, K.; Dik, J. The role of smalt in complex pigment mixtures in Rembrandt's Homer 1663: combining MA-XRF imaging, microanalysis, paint reconstructions and OCT. *Herit. Sci.* **2020**, *8* (1), 90. DOI: 10.1186/s40494-020-00429-5.
(13) Janssens, K.; Van der Snickt, G.; Vanmeert, F.; Legrand, S.; Nuyts, G.; Alfeld, M.; Monico, L.; Anaf, W.; De Nolf, W.; Vermeulen, M.; et al. Non-Invasive and Non-Destructive Examination of Artistic Pigments, Paints, and Paintings by Means of X-Ray Methods. *Top. Curr. Chem.* **2016**, *374* (6), 81. DOI: 10.1007/s41061-016-0079-2.

(14) Sabatini, F.; Degano, I. Analysis of Natural and Synthetic Organic Lakes and Pigments by Chromatographic and Mass Spectrometric Techniques. In *Analytical Chemistry for the Study of Paintings and the Detection of Forgeries*, Colombini, M. P., Degano, I., Nevin, A. Eds.; Springer International Publishing, 2022; pp 247-287.
(15) Degano, I.; Tognotti, P.; Kunzelman, D.; Modugno, F. HPLC-DAD and HPLC-ESI-Q-ToF characterisation of early 20th century lake and organic pigments from Lefranc archives. *Herit. Sci.* **2017**, *5* (1), 7, journal article. DOI: 10.1186/s40494-017-0120-y.
(16) Degano, I.; Ribechini, E.; Modugno, F.; Colombini, M. P. Analytical Methods for the Characterization of Organic Dyes in Artworks and in Historical Textiles. *Applied Spectroscopy Reviews* **2009**, *44* (5), 363-410. DOI: 10.1080/05704920902937876.
(17) Ferreira, E. S. B.; Heeren, R. M. A.; van den Berg, K. J.; Maines, C.; Sutherland, K.; Higgitt, C. Mass Spectrometry of Art and Cultural Heritage. *Int. J. Mass spectrom.* **2009**, *284* (1–3), 1. DOI: http://dx.doi.org/10.1016/j.ijms.2009.04.006.
(18) Sundberg, B. N.; Pause, R.; van der Werf, I. D.; Astefanei, A.; van den Berg, K. J.; van Bommel, M. R. Analytical approaches for the characterization of early synthetic organic pigments for artists' paints. *Microchem. J.* **2021**, *170*, 106708. DOI: https://doi.org/10.1016/j.microc.2021.106708.
(19) *Organic Mass Spectrometry in Art and Archaeology*; John Wiley & Sons, Ltd, 2009. DOI: 10.1002/9780470741917.
(20) Astefanei, A.; van Bommel, M.; Corthals, G. L. Surface Acoustic Wave Nebulisation Mass Spectrometry for the Fast and Highly Sensitive Characterisation of Synthetic Dyes in Textile Samples. *J. Am. Soc. Mass. Spectrom.* **2017**, *28* (10), 2108-2116. DOI: 10.1007/s13361-017-1716-x.
(21) Astefanei, A.; van den Berg, K. J.; Burnstock, A.; Corthals, G. Surface Acoustic Wave Nebulization–Mass Spectrometry as a New Tool to Investigate the Water Sensitivity Behavior of 20th Century Oil Paints. *J. Am. Soc. Mass. Spectrom.* **2021**, *32* (2), 444-454. DOI: 10.1021/jasms.0c00272.
(22) Sandström, E.; Vettorazzo, C.; Mackay, C. L.; Troalen, L. G.; Hulme, A. N. Development and Application of Desorption Electrospray Ionization Mass Spectrometry for Historical Dye Analysis. *Anal. Chem.* **2023**, *95* (11), 4846-4854. DOI: 10.1021/acs.analchem.2c03281.
(23) Alvarez-Martin, A.; Cleland, T. P.; Kavich, G. M.; Janssens, K.; Newsome, G. A. Rapid Evaluation of the Debromination Mechanism of Eosin in Oil Paint by Direct Analysis in Real Time and Direct Infusion-Electrospray Ionization Mass Spectrometry. *Anal. Chem.* **2019**, *91* (16), 10856-10863. DOI: 10.1021/acs.analchem.9b02568.
(24) Claes, B. S. R.; Krestensen, K. K.; Yagnik, G.; Grgic, A.; Kuik, C.; Lim, M. J.; Rothschild, K. J.; Vandenbosch, M.; Heeren, R. M. A. MALDI-IHC-Guided In-Depth Spatial Proteomics: Targeted and Untargeted MSI Combined. *Anal. Chem.* **2023**, *95* (4), 2329-2338. DOI: 10.1021/acs.analchem.2c04220.
(25) Condina, M. R.; Mittal, P.; Briggs, M. T.; Oehler, M. K.; Klingler-Hoffmann, M.; Hoffmann, P. Egg White as a Quality Control in Matrix-Assisted Laser Desorption/Ionization Mass Spectrometry Imaging (MALDI-MSI). *Anal. Chem.* **2019**, *91* (23), 14846-14853. DOI: 10.1021/acs.analchem.9b03091.
(26) Cillero-Pastor, B.; Heeren, R. M. A. Matrix-Assisted Laser Desorption Ionization Mass Spectrometry Imaging for Peptide and Protein Analyses: A Critical Review of On-Tissue Digestion. *Journal of Proteome Research* **2014**, *13* (2), 325-335. DOI: 10.1021/pr400743a.
(27) Wang, J.; Zhao, J.; Nie, S.; Xie, M.; Li, S. MALDI mass spectrometry in food carbohydrates analysis: A review of recent researches. *Food Chem.* **2023**, *399*, 133968. DOI: https://doi.org/10.1016/j.foodchem.2022.133968.
(28) Cillero-Pastor, B.; Cuypers, E. Sample Preparation of Biological Tissues for MALDI-MSI. In *MALDI Mass Spectrometry Imaging: From Fundamentals to Spatial Omics*, Porta Siegel, T. Ed.; The Royal Society of Chemistry, 2021; p 0.
(29) Geldof, M.; de Keijzer, M.; van Bommel, M.; Pilz, K.; Salvant, J.; van Keulen, H.; Megens, L. Van Gogh's geranium lake. In *Van Gogh's Studio Practice*, Vellekoop, M., Jansen, L., Geldof, M., Hendriks, H., de Tagle, A. Eds.; Mercatorfonds, 2013.

(30) *Vincent van Gogh: The Letters. The complete, illustrated and annotated edition*; Thames & Hudson.
(31) Welcomme, E.; Walter, P.; Bleuet, P.; Hodeau, J. L.; Dooryhee, E.; Martinetto, P.; Menu, M. Classification of lead white pigments using synchrotron radiation micro X-ray diffraction. *Appl. Phys. A* **2007**, *89* (4), 825-832. DOI: 10.1007/s00339-007-4217-0.
(32) *Van Gogh's Studio Practice*; Mercatorfonds, 2013.
(33) Anselmi, C.; Capitani, D.; Tintaru, A.; Doherty, B.; Sgamellotti, A.; Miliani, C. Beyond the color: A structural insight to eosin-based lakes. *Dyes Pigm.* **2017**, *140*, 297-311. DOI: http://dx.doi.org/10.1016/j.dyepig.2017.01.046.
(34) Alvarez-Martin, A.; Trashin, S.; Cuykx, M.; Covaci, A.; De Wael, K.; Janssens, K. Photodegradation mechanisms and kinetics of Eosin-Y in oxic and anoxic conditions. *Dyes Pigm.* **2017**, *145* (Supplement C), 376-384. DOI: https://doi.org/10.1016/j.dyepig.2017.06.031.
(35) Sabatini, F.; Eis, E.; Degano, I.; Thoury, M.; Bonaduce, I.; Lluveras-Tenorio, A. The issue of eosin fading: A combined spectroscopic and mass spectrometric approach applied to historical lakes. *Dyes Pigm.* **2020**, *180*, 108436. DOI: https://doi.org/10.1016/j.dyepig.2020.108436.
(36) Groeneveld, I.; Ariese, F.; Somsen, G. W.; van Bommel, M. R. Gas-permeable liquid-core waveguide coupled to LC-MS for studying the influence of oxygen on photodegradation processes. *Journal of Photochemistry and Photobiology A: Chemistry* **2023**, *441*, 114685. DOI: https://doi.org/10.1016/j.jphotochem.2023.114685.
(37) Sabatini, F.; Giugliano, R.; Degano, I. Photo-oxidation processes of Rhodamine B: A chromatographic and mass spectrometric approach. *Microchem. J.* **2018**, *140*, 114-122. DOI: https://doi.org/10.1016/j.microc.2018.04.018.
(38) Radepont, M.; Coquinot, Y.; Janssens, K.; Ezrati, J.-J.; de Nolf, W.; Cotte, M. Thermodynamic and experimental study of the degradation of the red pigment mercury sulfide. *J. Anal. At. Spectrom.* **2015**, *30* (3), 599-612, 10.1039/C4JA00372A. DOI: 10.1039/C4JA00372A.
(39) Yu, J.; Warren, W. S.; Fischer, M. C. Visualization of vermilion degradation using pump-probe microscopy. *Science Advances* **2019**, *5* (6), eaaw3136. DOI: doi:10.1126/sciadv.aaw3136.
(40) Keune, K.; Boon, J. J. Analytical Imaging Studies Clarifying the Process of the Darkening of Vermilion in Paintings. *Anal. Chem.* **2005**, *77* (15), 4742-4750. DOI: 10.1021/ac048158f.
(41) Chua, L.; Banas, A.; Banas, K. Comparison of ATR-FTIR and O-PTIR Imaging Techniques for the Characterisation of Zinc-Type Degradation Products in a Paint Cross-Section. *Molecules* **2022**, *27* (19). DOI: 10.3390/molecules27196301 From NLM.
(42) Claro, A.; Melo, M. J.; Schäfer, S.; de Melo, J. S. S.; Pina, F.; van den Berg, K. J.; Burnstock, A. The use of microspectrofluorimetry for the characterization of lake pigments. *Talanta* **2008**, *74* (4), 922-929. DOI: http://dx.doi.org/10.1016/j.talanta.2007.07.036.
(43) De Meyer, S.; Vanmeert, F.; Vertongen, R.; Van Loon, A.; Gonzalez, V.; Delaney, J.; Dooley, K.; Dik, J.; Van der Snickt, G.; Vandivere, A.; et al. Macroscopic x-ray powder diffraction imaging reveals Vermeer’s discriminating use of lead white pigments in Girl with a Pearl Earring. *Science Advances* **2019**, *5* (8), eaax1975. DOI: doi:10.1126/sciadv.aax1975.
(44) DeNolf, W.; Vanmeert, F.; Janssens, K. XRDUA: crystalline phase distribution maps by two-dimensional scanning and tomographic (micro) X-ray powder diffraction. *J. Appl. Crystallogr.* **2014**, *47*, 1107-1117. DOI: https://doi.org/10.1107/S1600576714008218.
(45) Haartmans, M. J. J.; Claes, B. S. R.; Emanuel, K. S.; Tuijthof, G. J. M.; Heeren, R. M. A.; Emans, P. J.; Cillero-Pastor, B. Sample preparation for lipid analysis of intra-articular adipose tissue by using matrix-assisted laser desorption/ionization imaging. *Anal. Biochem.* **2023**, *662*, 115018. DOI: https://doi.org/10.1016/j.ab.2022.115018.
(46) Fernández, R.; Garate, J.; Martín-Saiz, L.; Galetich, I.; Fernández, J. A. Matrix Sublimation Device for MALDI Mass Spectrometry Imaging. *Anal. Chem.* **2019**, *91* (1), 803-807. DOI: 10.1021/acs.analchem.8b04765.

(47) Alvarez-Martin, A.; Janssens, K. Protecting and stimulating effect on the degradation of eosin lakes. Part 1: Lead white and cobalt blue. *Microchem. J.* **2018**, *141*, 51-63. DOI: https://doi.org/10.1016/j.microc.2018.05.005.
(48) Van Nuffel, S.; Elie, N.; Yang, E.; Nouet, J.; Touboul, D.; Chaurand, P.; Brunelle, A. Insights into the MALDI Process after Matrix Deposition by Sublimation Using 3D ToF-SIMS Imaging. *Anal. Chem.* **2018**, *90* (3), 1907-1914. DOI: 10.1021/acs.analchem.7b03993.
(49) Good, C. J.; Neumann, E. K.; Butrico, C. E.; Cassat, J. E.; Caprioli, R. M.; Spraggins, J. M. High Spatial Resolution MALDI Imaging Mass Spectrometry of Fresh-Frozen Bone. *Anal. Chem.* **2022**, *94* (7), 3165-3172. DOI: 10.1021/acs.analchem.1c04604.
(50) Xie, H.; Wu, R.; Hung, Y. L. W.; Chen, X.; Chan, T. W. D. Development of a Matrix Sublimation Device with Controllable Crystallization Temperature for MALDI Mass Spectrometry Imaging. *Anal. Chem.* **2021**, *93* (16), 6342-6347. DOI: 10.1021/acs.analchem.1c00260.
(51) Alvarez-Martin, A.; Newsome, G. A.; Janssens, K. High-Resolution Mass Spectrometry and Nontraditional Mass Defect Analysis of Brominated Historical Pigments. *Anal. Chem.* **2021**, *93* (44), 14851-14858. DOI: 10.1021/acs.analchem.1c03815.
(52) Pirok, B. W. J.; Moro, G.; Meekel, N.; Berbers, S. V. J.; Schoenmakers, P. J.; van Bommel, M. R. Mapping degradation pathways of natural and synthetic dyes with LC-MS: Influence of solvent on degradation mechanisms. *J. Cult. Herit.* **2019**, *38*, 29-36. DOI: https://doi.org/10.1016/j.culher.2019.01.003.
(53) Arbeloa, E. M.; Previtali, C. M.; Bertolotti, S. G. Photochemical study of Eosin-Y with PAMAM dendrimers in aqueous solution. *J. Lumin.* **2016**, *180*, 369-375. DOI: http://dx.doi.org/10.1016/j.jlumin.2016.08.017.
(54) Kimura, K.; Miwa, T.; Imamura, M. Photochemical debromination of eosin in basic methanolic solution. *Chemical Communications (London)* **1968**, (24), 1619-1621, 10.1039/C19680001619. DOI: 10.1039/C19680001619.
(55) Sabatini, F.; Degano, I.; Colombini, M. P. Development of a method based on high-performance liquid chromatography coupled with diode array, fluorescence, and mass spectrometric detectors for the analysis of eosin at trace levels. *SEPARATION SCIENCE PLUS* **2020**, *3* (6), 207-215. DOI: https://doi.org/10.1002/sscp.202000002.
(56) Pirok, B. W. J.; Moro, G.; Meekel, N.; Berbers, S. V. J.; Schoenmakers, P. J.; van Bommel, M. R. Mapping degradation pathways of natural and synthetic dyes with LC-MS: Influence of solvent on degradation mechanisms. *J. Cult. Herit.* **2019**. DOI: https://doi.org/10.1016/j.culher.2019.01.003.
(57) Bellal, B.; Trari, M.; Afalfiz, A. Synthesis and characterization of CdS/CuAl2O4 core–shell: application to photocatalytic eosin degradation. *Applied Nanoscience* **2015**, *5* (6), 673-680. DOI: 10.1007/s13204-014-0363-9.
(58) Bhattacharjee, A.; Ahmaruzzaman, M. CuO nanostructures: facile synthesis and applications for enhanced photodegradation of organic compounds and reduction of p-nitrophenol from aqueous phase. *RSC Advances* **2016**, *6* (47), 41348-41363, 10.1039/C6RA03624D. DOI: 10.1039/C6RA03624D.
(59) Qiao, Z.; Lissel, F. MALDI Matrices for the Analysis of Low Molecular Weight Compounds: Rational Design, Challenges and Perspectives. *Chem Asian J* **2021**, *16* (8), 868-878. DOI: 10.1002/asia.202100044.
(60) Fieberg, J. E.; Knutås, P.; Hostettler, K.; Smith, G. D. "Paintings Fade Like Flowers": Pigment Analysis and Digital Reconstruction of a Faded Pink Lake Pigment in Vincent van Gogh's Undergrowth with Two Figures. *Appl. Spectrosc.* **2017**, *71* (5), 794-808. DOI: doi:10.1177/0003702816685097.
(61) Burnstock, A.; Lanfear, I.; Berg, K. v. d.; Carlyle, L.; Clarke, M.; Hendriks, E.; Kirby, J. Comparison of the fading and surface deterioration of red lake pigments in six paintings by Vincent van Gogh with artificially aged paint reconstructions. *Preprints of the 14th Triennial Meeting of the ICOM Committee for Conservation, The Hague* **2005**, 459-466.

(62) Kirchner, E.; van der Lans, I.; Ligterink, F.; Geldof, M.; Ness Proano Gaibor, A.; Hendriks, E.; Janssens, K.; Delaney, J. Digitally reconstructing Van Gogh's Field with Irises near Arles. Part 2: Pigment concentration maps. *Color Res. Appl.* **2018**, *43* (2), 158-176. DOI: doi:10.1002/col.22164.
(63) Kirchner, E.; van der Lans, I.; Ligterink, F.; Geldof, M.; Megens, L.; Meedendorp, T.; Pilz, K.; Hendriks, E. Digitally reconstructing Van Gogh's Field with Irises near Arles part 3: Determining the original colors. *Color Res. Appl.* **2018**, *43* (3), 311-327. DOI: doi:10.1002/col.22197.
(64) Geldof, M.; Proaño Gaibor, A. N.; Ligterink, F.; Hendriks, E.; Kirchner, E. Reconstructing Van Gogh's palette to determine the optical characteristics of his paints. *Herit. Sci.* **2018**, *6* (1), 17, journal article. DOI: 10.1186/s40494-018-0181-6.

## Graphical abstract

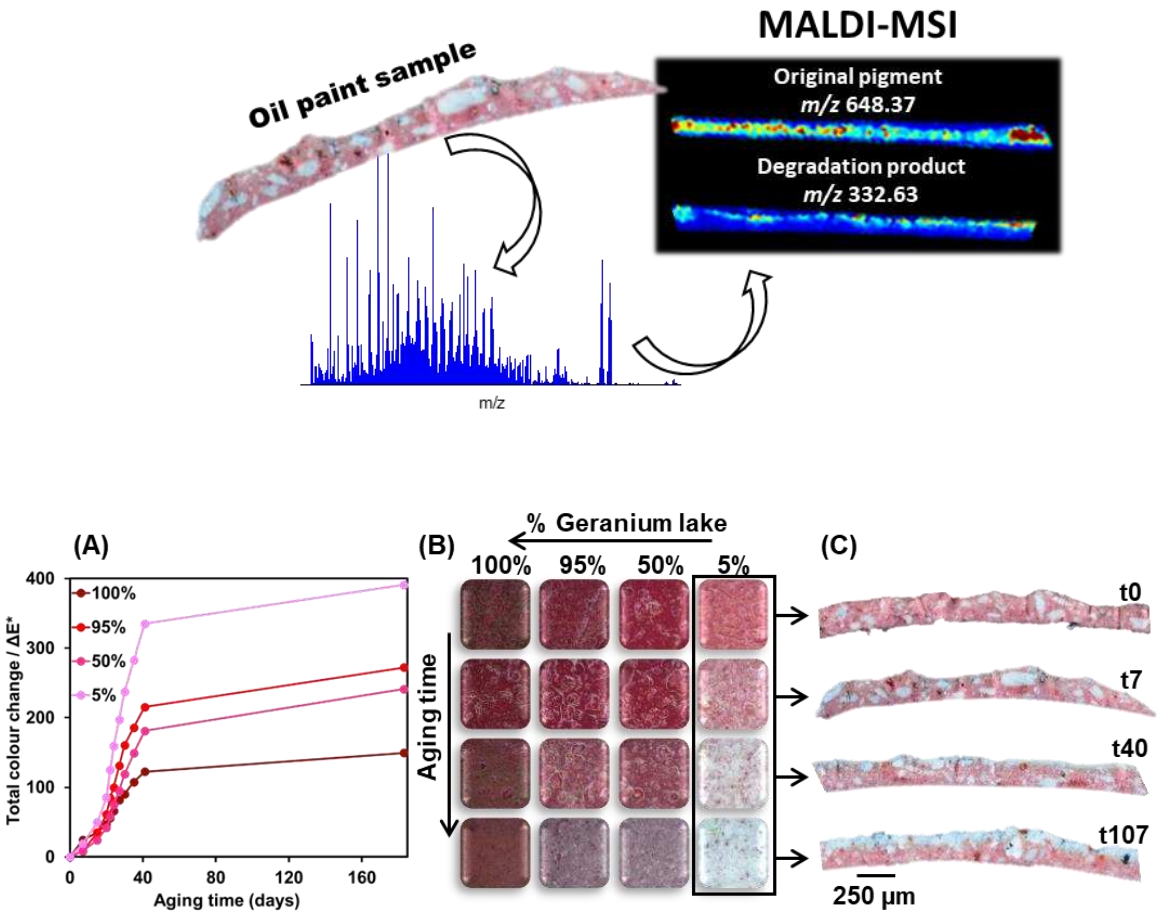


**Figure 1. (A)** Total color change ($\Delta E^*$) during the aging experiment of paint models containing different mass ratios of geranium lake and lead white pigments. **(B)** Optical photographs of the surface of the paint models during aging. **(C)** Optical microscopy of non-embedded paint cross sections correspoinding to a sample containing 5% of geranium lake over time.

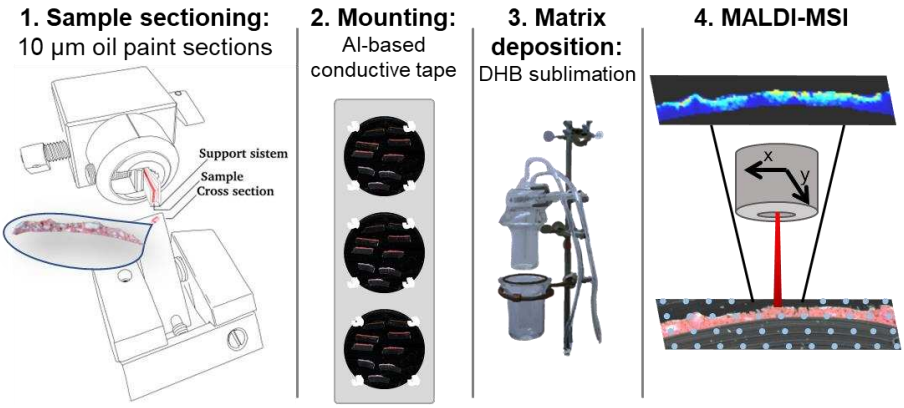


**Scheme 1.** Workflow depicting the sample preparation used for MALDI-MSI of oil paint samples: (1) Sample preparation, (2) Mounting, (3) Matrix deposition and (4) MALDI-MSI analysis.

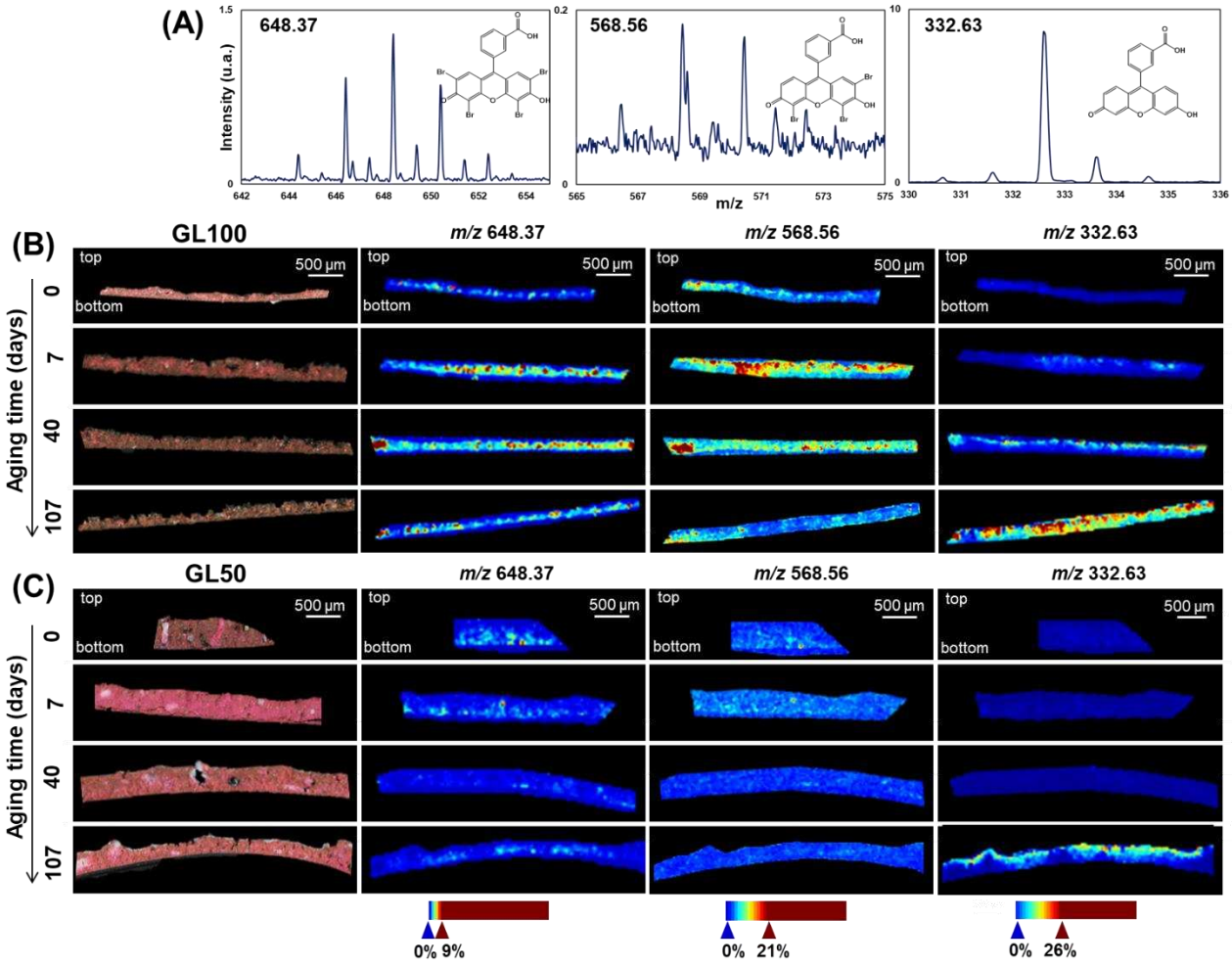


**Figure 2.** **(A)** Average full MS spectra of eosin (*m/z* 648.371 $[C_{20}H_9O_5Br_4]^+$) and its degradation products (*m/z* 568.561, $[C_{20}H_{10}O_5Br_3]^+$ and 332.630 $[C_{20}H_{13}O_5]^+$). **(B-C)** Optical images of paint cross sections and 10 µm spatial resolution ion images of *m/z* 648.371, *m/z* 568.561 and *m/z* 332.630 of samples GL100 and GL50. (See Figure S5 for the full data set of samples analysed).

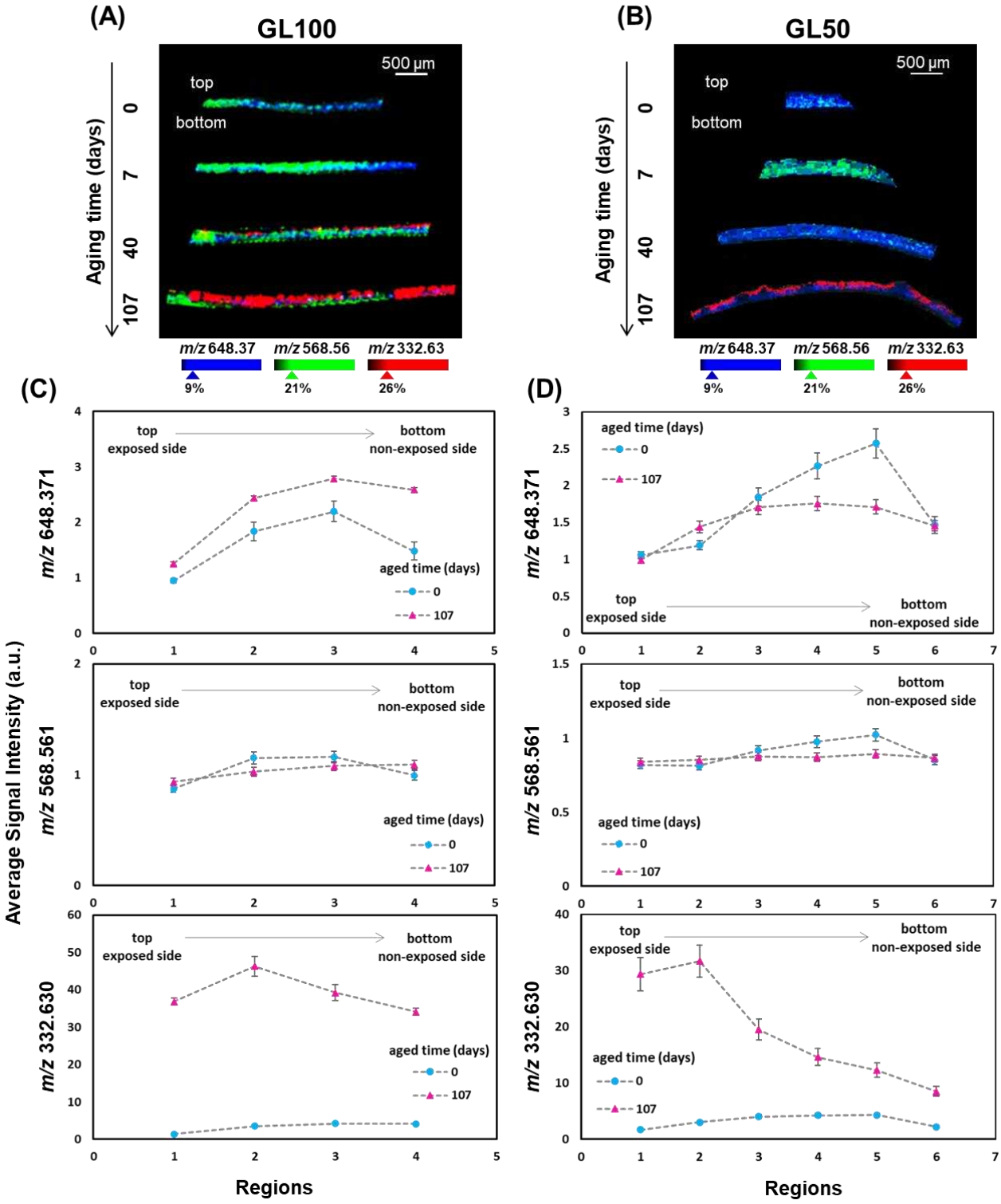


**Figure 3.** Ion images showing the spatial distribution of three representative ions: *m/z* 648.371, *m/z* 568.561 and *m/z* 332.630 in samples **(A)** GL100 and **(B)** GL50. **(C-D)** Variation in average signal intensity in depth. Error bars depict standard deviation of n = 3 replicates. The average signal intensity was determined from the average mass spectra of 4 to 6 regions in the samples (see Figure S6).